ICARUS 79, 23–37 (1989)

The Surface Albedo Distribution of Pluto

MARC W. BUIE[1] AND DAVID J. THOLEN

Institute for Astronomy, University of Hawaii, 2680 Woodlawn Drive, Honolulu, Hawaii 96822

Received April 19, 1988; revised September 15, 1988

We present a new model for the surface albedo distribution of Pluto that fits absolute photometry spanning 1954 to 1986. We found two distinct configurations that fit out-of-eclipse photometry equally well. Each set of model parameters contains two spots near the equator and two polar caps. The two sets differ primarily in the equatorial spots; one set has two dark spots while the other has one dark and one bright spot. To first order, the equatorial spots generate the rotational lightcurve and the polar caps produce the orbital lightcurve (frequently referred to as the secular dimming). However, these effects are not separable as previously thought. We compared these models with available mutual event data and found that the agreement is good. Through the end of 1987 the two models predict similar event lightcurves but beginning in 1988 they differ quite markedly. One of our recent mutual event observations made on 1988 January 13 UT is in agreement with only one of the equatorial spot configurations: the model with one bright and one dark spot.

INTRODUCTION

Twenty years after the discovery of Pluto, Walker and Hardie (1955) found that the brightness of Pluto varies, thus allowing them to determine a rotational period. Since that time, observations by Hardie (1965), Andersson and Fix (1973), Neff *et al.* (1974), Binzel and Mulholland (1984), and Tholen and Tedesco (1988) have shown that the lightcurve varies; the amplitude of the lightcurve has increased and the mean brightness has decreased.

Lacis and Fix (1972), Andersson and Fix (1973), and Renschen (1977) explained the lightcurve of Pluto in terms of the changing viewing aspect caused by a high obliquity coupled with a fixed surface albedo distribution. Their explanations provided the first crude pole position for Pluto and a very rough idea of the contrast that exists on the surface. All of this work was severely hampered by the short time interval spanned by the observations (~8% of Pluto's orbit) and the quality of the data set.

A decade later and after the discovery of Pluto's satellite, Marcialis (1983, 1988, hereafter referred to as the TSM, or two-spot model) once again attempted to explain the observed lightcurve. By that time, additional photometry and an improved pole orientation were available. Using two dark circular spots on the surface of Pluto, Marcialis reproduced the changing shape and amplitude of the rotational lightcurve. Marcialis also concluded that a dark equatorial band could account for the decrease in mean brightness.

Many questions still remain that we will address in this paper. Can a fixed surface albedo distribution reproduce the lightcurve of Pluto? If so, is the assumption of a permanent surface albedo distribution reasonable? How much contrast is there between different regions on the surface? In this paper we present new observations and an improved model that fits the observed lightcurve of Pluto from 1954 to 1986.

[1] Current address: Space Telescope Science Institute, 3700 San Martin Dr., Baltimore, MD 21218.

0019-1035/89 $3.00

TABLE I

PHOTOMETRIC OBSERVATIONS OF PLUTO IN 1986

JD of observation	B mag	σ	Observer(s)	Telescope
2446414.14441	14.8450	0.0028	Tholen	UH 2.24-m
2446428.12837	14.8058	0.0045	Tholen	UH 2.24-m
2446429.13537	14.7087	0.0075	Tholen	UH 2.24-m
2446433.13147	14.8460	0.0082	Tholen	UH #1 0.61-m
2446442.10859	14.6984	0.0023	Tholen	UH 2.24-m
2446443.07966	14.7992	0.0028	Tholen	UH 2.24-m
2446443.12528	14.8058	0.0032	Tholen	UH 2.24-m
2446444.05130	15.0023	0.0034	Tholen and Buie	UH 2.24-m
2446444.11065	15.0061	0.0033	Tholen and Buie	UH 2.24-m
2446445.05413	14.9229	0.0046	Buie and Tholen	UH 2.24-m
2446445.14423	14.9217	0.0043	Tholen and Buie	UH 2.24-m
2446446.11899	14.8260	0.0009	Tholen	UH 2.24-m
2446449.05752	14.7652	0.0122	Buie	UH #1 0.61-m
2446496.11304	14.8943	0.0185	Tholen and Lark	UH #1 0.61-m
2446498.10231	14.7303	0.0051	Tholen	UH #1 0.61-m
2446499.07867	14.6661	0.0058	Tholen	UH #1 0.61-m
2446500.07776	14.6481	0.0070	Tholen	UH #1 0.61-m
2446501.07308	14.8381	0.0062	Tholen	UH #1 0.61-m
2446502.09032	14.9126	0.0066	Tholen	UH #1 0.61-m
2446503.05411	14.7784	0.0053	Tholen	UH #1 0.61-m
2446509.98459	14.7362	0.0012	Tholen	UH 2.24-m
2446510.11683	14.7307	0.0019	Tholen	UH 2.24-m
2446514.10574	14.8777	0.0032	Tholen	UH 2.24-m
2446523.91417	14.6943	0.0062	Buie	UH #1 0.61-m
2446539.87000	14.8529	0.0028	Tholen	UH 2.24-m
2446539.97810	14.8624	0.0045	Tholen	UH 2.24-m
2446540.09619	14.8689	0.0020	Tholen	UH 2.24-m
2446540.87147	14.7897	0.0057	Tholen	UH 2.24-m
2446541.93138	14.6909	0.0012	Tholen	UH 2.24-m
2446542.89250	14.6703	0.0030	Tholen	UH 2.24-m
2446543.03821	14.6620	0.0030	Tholen	UH 2.24-m
2446543.89733	14.5845	0.0047	Tholen	UH 2.24-m
2446544.82196	14.5797	0.0079	Tholen	UH 2.24-m
2446544.91591	14.5991	0.0030	Tholen	UH 2.24-m
2446578.01192	14.8838	0.0090	Tholen	UH #1 0.61-m
2446578.89047	14.8715	0.0053	Tholen	UH #1 0.61-m
2446579.89957	14.7440	0.0040	Tholen	UH #1 0.61-m
2446589.91007	14.7021	0.0041	Tholen	UH #1 0.61-m
2446590.90150	14.8996	0.0048	Tholen	UH #1 0.61-m
2446591.90397	14.8573	0.0045	Tholen	UH #1 0.61-m
2446608.78362	14.6768	0.0014	Tholen	UH 2.24-m
2446608.97190	14.7103	0.0031	Tholen	UH 2.24-m
2446619.80110	14.7544	0.0021	Tholen	UH 2.24-m
2446620.85141	14.6649	0.0019	Tholen	UH 2.24-m

OBSERVATIONS AND DATA

Table I lists the new data that we obtained on Mauna Kea with the University of Hawaii 2.24-m and #1 0.61-m telescopes. The times listed in Table I are the Julian dates corresponding to the time of observation. The magnitude reported is the apparent Johnson B magnitude. All observations were made differentially with respect to one of two local comparison stars. Prior to opposition (late April), we used the star called "1986 Primary," and, after opposition, "1985 Primary" was used. These two stars were selected primarily for use during mutual event observations (Tholen 1985). The Johnson magnitudes for these stars were, in turn, determined differen-

TABLE II

SUMMARY OF PLUTO PHOTOMETRY

Year	Points	Filter	Average sub-Earth latitude (°)	Observer(s)	Reference
1933	20	P†	−55.3	Baade	Baade (1934)
1953	6	V	−55.4	Kuiper	Walker and Hardie (1955)
* 1954	6	V	−54.6	Walker	Walker and Hardie (1955)
* 1955	15	Open‡	−54.0	Walker, Hardie	Walker and Hardie (1955)
* 1964	14	V	−44.6	Hardie	Marcialis (1983, 1988)
1966	5	V	−41.5	Kiladze	Kiladze (1967)
* 1972	18	V	−30.5	Andersson	Andersson and Fix (1973)
1973	28	V	−29.5	Neff	Neff *et al.* (1974)
* 1975	12	V	−24.9	Lane, Neff, Fix	Lane *et al.* (1974)
1978	21	U,B,V	−20.5	Abramenko *et al.*	Abramenko *et al.* (1981)
* 1980	26	B	−15.5	Tholen, Tedesco	Tholen and Tedesco (1988)
* 1981	35	B	−13.4	Tholen, Tedesco	Tholen and Tedesco (1988)
1981	63	U,B,V	−15.0	Lyutyi, Tarashchuk	Lyutyi and Tarashchuk (1982)
* 1982	27	B	−11.0	Binzel, Mulholland	Binzel and Mulholland (1984)
* 1982	63	B	−13.4	Tholen	Tholen and Tedesco (1988)
* 1983	27	B	−11.0	Binzel, Mulholland	Binzel and Mulholland (1984)
* 1983	20	B	−9.0	Tholen	Tholen and Tedesco (1988)
* 1984	27	B	−7.1	Binzel	Binzel, private communication
* 1986	44	B	−3.0	Tholen, Buie, Lark	this work

Note. An asterisk before the date indicates which data were used to constrain the model.
† P stands for photographic magnitude.
‡ Open stands for an unfiltered, i.e., "open," detector.

tially with respect to SAO 120107, which we have defined to have $B = 9.8966$, $V = 9.2400$, and $(B - V) = 0.6566$. The tabulated uncertainties represent one standard deviation of only the Pluto photometry. The error in the transformation to the standard system has not been included, pending finalization of the photometric system. As such, there may be a systematic error of up to a few thousandths of a magnitude between the data obtained before and after opposition.

Table II summarizes the available photometry of Pluto through the end of 1986. The first column indicates the data that we modeled. We excluded some data sets from the fit, as explained below, because of excessive random or systematic errors. However, we included the data set from 1955 despite its systematic error due to the pau-

city of older observations. These data were obtained through an ultraviolet blocking filter whereas the 1954 data were obtained through a Johnson V filter, leading to a poor match of photometric systems. We found that a 0.042-mag correction, when added to the data, removes all of the small vertical offset between the 1954 and 1955 data. Because the sub-Earth latitude was changing very slowly, there should have been very little change in the lightcurve between the two epochs. We note that Marcialis (1983, 1988) also applied a similar correction to the 1955 data but his value was 0.024 mag.

The 1933 data of Baade (1934) were obtained photographically, and as such probably have random errors in excess of 0.1 mag, which renders the data too crude for our purposes. Kuiper's 1953 observations (Walker and Hardie 1955) were excluded because of the lack of error bars on the data. In addition, the observations were not very consistent with the Walker and Hardie (1955) measurements. Without knowing how to weight the data against other data sets, we felt that the data should not be included in the model fit. We did attempt to trace the origins of the Kuiper data, but to no avail. Walker and Hardie (1955) mention that the Kuiper data they presented were from a larger collection that Kuiper had not yet made public. At our request, E. Whitaker searched the Kuiper archives at the University of Arizona, but he was not able to find any mention of the "missing" Pluto photometry. A similar request made to R. Hardie by R. Marcialis (private communication) in 1981 yielded no positive results either.

Kiladze's 1966 data (Kiladze 1967) are totally inconsistent with the Hardie data from 1964. Several other authors have speculated that Kiladze performed only differential photometry and adjusted his zero point so that his data matched the 1954–1955 data. Lyutyi and Tarashchuk (1982) dismissed this possibility, claiming that Kiladze did not publish any data of his own. The obvious discrepancy is due to the fact that Lyutyi and Tarashchuk referenced Kiladze (1966) which does not contain data, rather than Kiladze (1967), which does.

The 1973 data set was excluded from the fit because it is inconsistent with the orbital lightcurve and the rotational lightcurves defined by the other good data sets near the same epoch. We were surprised at this inconsistency since the data should be of high quality. The data Neff collected in 1973 were primarily intended to disprove a shorter photometric period proposed by Kiladze (1966). The data span 4 consecutive nights within which "high" time resolution photometry was obtained. The mean of each individual night of observation is close to the final models. However, the slope of the lightcurve within a single night is very different from the lightcurves measured in 1972 and 1975. Most of the other lightcurves used in this analysis are comprised of many observations which were spread out over many more nights. Such a spread in the observations provides data which are less susceptible to systematic errors within a night and also provides a better measure of the scatter of the observations. For these reasons we excluded the 1973 Neff data from the model fit.

The Abramenko 1978 data set was obtained via some sort of television system with dubious linearity and therefore was eliminated. Last, the Lyutyi and Tarashchuk data were excluded because of large random errors (which, we note, led to their erroneous claim of detecting the first mutual events). In total, we modeled a 318-point subset of the full data set containing 461 points.

There is one important change from previous work in the way we present the data in this paper. In the past it has been customary to plot magnitude versus lightcurve phase, a simple quantity the computation of which requires only a lightcurve period and an epoch. There are important limitations to this technique. A lightcurve period is a good approximation of the rotational period

over the interval of observation when the lightcurve extrema occur at the same phase for all sub-Earth latitudes. In the case of Pluto, the sub-Earth latitude has changed substantially since the first lightcurve measurements. It is quite possible that the albedo features on the surface could cause a significant drift of the lightcurve extrema over the time of observation.

Because we now have an independent determination of the rotational period, we no longer need to use, or even solve for, the lightcurve phase. We can now compute a quantity which corrects for all effects due to viewing geometry: the east longitude of the sub-Earth point, where we define 0° long to be the sub-Charon point. By using longitude, parallax no longer distorts the shape of the lightcurve and the spot locations are completely decoupled from the determination of the primary independent variable. This step also removes the false structure from the χ^2 surface that is due to the irregular sampling interval.

The orbit for Pluto, taken from the *Astronomical Almanac* (cf. 1988 vol., Sect. E), provides the distance and phase angle information. The orbit of Charon (Tholen and Buie 1987) provides the latitude and longitude by assuming Pluto is locked in a 1 : 1 spin–orbit resonance with Charon (orbital period of Charon equals the rotational period of Pluto and eccentricity of Charon's orbit is zero). For consistency with our previous work on Pluto, we define the north pole to be parallel with the spin angular momentum vector of Pluto (rather than antiparallel as required by the IAU definition).

This latest orbit for the satellite provides much better information about the orientation of Pluto over the time span of the data base than that previously available. In contrast, Marcialis' TSM relied on a polynomial approximation to the instantaneous plane-of-sky inclination determined by Harrington and Christy (1981). Primarily intended only for dates near the onset of mutual events, this formula does not work well away from the epoch of the polynomial.

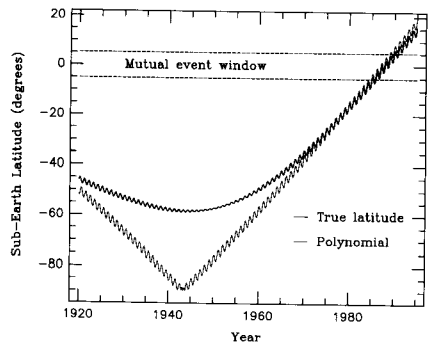

FIG. 1. Comparison of the Harrington and Christy (1981) polynomial for the sub-Earth latitude and a full orbital calculation based on the satellite orbit of Tholen and Buie (1987). The fine structure on the curves is due to the annual motion of the Earth. As we would expect from Pluto's obliquity, the amplitude is largest when the Earth passes through the equator of Pluto. The mutual event window indicates when events can be seen from the Earth.

For our modeling we have computed the true orientation of Pluto and Charon from their full orbital parameters. As shown in Fig. 1, the polynomial approximation differs quite strongly from the full calculation for dates prior to 1970. In particular, for the Walker and Hardie (1955) data, the error in the sub-Earth latitude is 12–15° depending on parallax. Such a large error casts serious doubts on the validity of the Marcialis TSM, with regard to understanding the orbital lightcurve. We note that our sub-Earth latitude calculations are good to about 2° for the 1950s, with the potential error decreasing as the sub-Earth point approaches 0° lat.

Before fitting a model to the data, we transformed the photometry to a Johnson B magnitude at the mean opposition distance (39.5 AU heliocentric, 38.5 geocentric) and zero degrees phase angle. We assumed a constant $(B - V)$ color for Pluto of 0.842 and a phase coefficient of 0.037 mag/deg. Tholen derived both quantities from an independent analysis of the 1980 to 1983 photometry.

An overview of the photometry of Pluto, presented in Fig. 2, shows a decrease in the overall brightness of the planet at all longi-

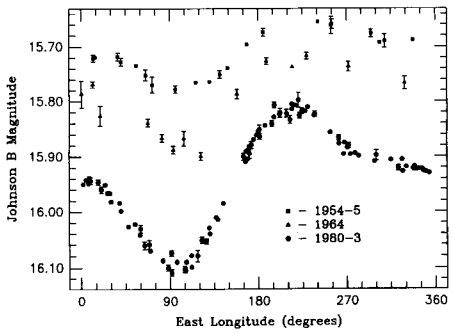

FIG. 2. A subset of the Pluto photometry. This shows the photometric data from 1954–1955, 1964, and 1980–1983 plotted as a function of the east longitude of the sub-Earth point. Note the change in shape, amplitude, and mean brightness since 1954. For clarity, all uncertainties less than 0.004 mag are not shown.

tudes as well as an increase in the lightcurve amplitude. The change in overall brightness is easier to see when plotted as a function of the sub-Earth latitude, shown in Fig. 3. For simplicity, we plot three longitudes from each lightcurve epoch. These longitudes correspond to the maximum of the lightcurve (MAX, 210°), the minimum (MIN, 100°), and the relatively constant portion of the lightcurve (SHELF, 350°). The orbital lightcurve clearly shows the rate at which the brightness change decreases as the sub-Earth point approaches the equator of Pluto. Note how the brightness has been essentially constant from 1980 to 1983 while the 1986 data show a slight upturn in brightness for MAX and MIN. It is the behavior of the lightcurve shown in Fig. 3 that we wish to model with a surface albedo distribution while still reproducing the rotational lightcurve.

MODEL

The basic assumption of our model is that the lightcurve is caused by static albedo patterns on the surface of Pluto. These patterns are treated as potentially overlapping circular spots. We have assumed throughout that Charon is a uniform sphere. The choice of circular spots minimizes the numerical computations and provides a more direct comparison between our results and the earlier TSM. We adopted the size and albedo of Charon and the size of Pluto as determined from the modeling of mutual event observations (Tholen and Buie 1987).

The reflected light from any given point on the surface is the bidirectional reflectance as defined in the surface reflectance theory of Hapke (1981). Computing the reflectance using Hapke's theory requires specifying two unknown quantities, the single scattering albedo, w, and the average particle phase function for the 180° scattering angle, $P(0)$. For reference, $P(0)$ is unity for isotropic scatterers. The advantage of using this theoretical formalism is that the reflected light is determined from fundamental quantities of the surface material which can, in principle, be constrained by laboratory measurements.

The Marcialis TSM uses normal reflectance and a linear limb-darkening coefficient to model the reflected light from the surface. The normal reflectance is the same as the bidirectional reflectance for zero degrees phase angle seen normal to the surface. In most cases, linear limb darkening provides a reasonable approximation to the limb darkening predicted from Hapke's theory. However, a precise correspondence between w and $P(0)$, and the TSM values does not exist. The goodness of fit between the two approaches should be similar for both treatments. In fact, the TSM is much

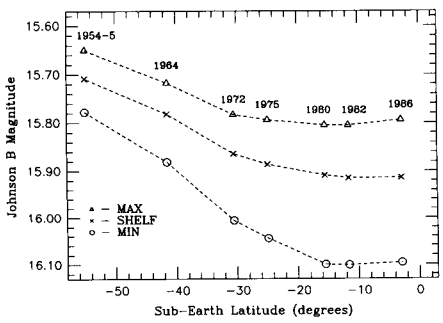

FIG. 3. The extrema of all lightcurves plotted as a function of the sub-Earth latitude. This gives a very clear picture of the orbital lightcurve.

simpler to compute, a definite advantage in its favor. Nonetheless, we feel that w and $P(0)$ are a much more useful set of model parameters because they relate to fundamental properties of the surface material. For instance, the value of w is constrained to lie between 0 and 1 by invoking conservation of energy. Also, from the value of $P(0)$ we can tell if a surface is forward- or backscattering; $P(0)$ less than one implies forward scattering particles while $P(0)$ greater than one implies back scattering particles.

Each spot on the surface adds five free parameters to the model. In addition to w and $P(0)$ there is the latitude and longitude of the center of the spot and its radius. For our modeling we used a weighted χ^2 where each residual is weighted by the reciprocal of the stated uncertainty squared. The model parameters that best fit the data were determined by a nonlinear least-squares technique based upon a simplex algorithm (cf. Caceci and Caceris 1984).

One difficulty with this algorithm was in ensuring physically allowable parameters. The algorithm requires an infinite χ^2 space to function properly, which in turn requires an infinite domain for each of the model parameters. In our case, some of the parameters have a noticeably finite domain. For instance, the single scattering albedo must lie between 0 and 1, inclusive. If the solution tends toward either end-point, the algorithm tries to compute a χ^2 using a value of w that is nonphysical.

To allow the program to continue, a value of χ^2 must be chosen when out-of-range parameters are encountered. Our first approach was to return a very large χ^2 when any parameter was out-of-range. In this case, the simplex will not converge on a solution. Instead, the solution will usually stop near the place where the parameter becomes invalid. We found that a better approach is to reflect the value about its physical limit, thus making the domain appear infinite. For example, a single scattering albedo of -0.1 is treated the same as 0.1 and, similarly, an albedo of 1.1 is treated as 0.9. Without this modification, the convergence time for the simplex algorithm was much longer.

RESULTS

We began our modeling by checking our calculations against those made previously by Marcialis. The albedo configuration proposed by Marcialis has two components, equatorial spots and latitudinal bands. Using the equatorial spots, we verified the ability of his model to reproduce the changing shape and amplitude of the lightcurve. We also verified that the latitudinal bands reproduce the orbital lightcurve. However, upon combining the two components, the model no longer fits the data. The presence of the bands severely reduced the amplitude of the rotational lightcurve. We discovered that the orbital and rotational lightcurves cannot be completely separated.

We investigated a number of different configurations in the search for the simplest way to match the observed lightcurve of Pluto. The first goal of the modeling was to explain the orbital lightcurve. One instructive case we considered was a single polar cap.

A single polar cap was not able to reproduce the shape of the orbital lightcurve. This configuration fits the total change in brightness between 1953 and 1986 but could not fit the photometry from 1964 and 1972. Furthermore, a single cap predicts the orbital lightcurve is not flat as our viewpoint crosses Pluto's equator.

By including a bright cap on each pole, the model reproduces the orbital lightcurve. As stated previously, the orbital and rotational lightcurves are not separable. However, the orbital lightcurve is independent of the rotational lightcurve in the model if we choose a longitude where the equatorial spots cannot be seen. For these special longitudes we can solve for the polar cap parameters independent of the equatorial spots. The procedure yields approxi-

TABLE III

SPOT MODEL PARAMETERS FOR SHELF

	Radius (km)	w	P(0)		
Pluto[a]	*1162.0*	0.776	2.1		
Charon[b]	*620.7*	*0.863*	*1.*		
Spot	Latitude	Longitude	Radius	w	P(0)
#1	−1.9	110.1	30.6	0.406	0.4
#2	−23.0	195.2	14.8	0.971	2.9
#3	81.4	195.6	59.4	0.999	2.2
#4	*South Pole*		44.2	1.000	1.5

Note. Both radii are based upon an assumed orbital radius of 19,800 km.
[a] Numbers on this line are unspotted properties of Pluto.
[b] Numbers for Charon are global properties.

mate values for the polar cap parameters which can then be used as starting points for the subsequent simultaneous fit involving all of the spots. The final model thus has four circular spots, yielding a total of 24 free parameters.

An important factor when using the simplex algorithm is the choice of starting point. From this point, the routine will search out the lowest χ^2 value that it can find by adjusting the model parameters in a direction that will decrease χ^2. The program converges on a solution when it cannot find a set of model parameters that yield a better χ^2. This criterion means that the solution will be a local minimum but not necessarily the absolute minimum or even the only minimum of similar depth. To check for consistency within the model and to search for multiple minima, we chose three different starting points.

The first step in determining a good starting point was to fit the orbital lightcurve using only the polar caps. This procedure resulted in three sets of parameters, one each that fit the MIN, MAX, and SHELF. To the polar cap configuration we added two equatorial spots at appropriate longitudes. For MIN, the two equatorial spots must be brighter than the background to reproduce the shelf and maximum of the rotational lightcurve. For SHELF, one equatorial spot must be darker than the background and one must be brighter. For MAX, there is a dark spot for the minimum and a dark spot for the shelf of the lightcurve.

From these three starting points the simplex algorithm began to search for the minimum χ^2. No minimum exists near the starting point for MIN. The model parameters quickly migrated toward those for SHELF. Both of the starting points for MAX and SHELF produced distinct and equally good fits to the data.

Tables III and IV summarize that model parameters for MAX and SHELF. The final model results are based on a 1° resolution integral over the surface. Italicized parameters were adopted from the model of Tholen and Buie (1987). The orbital radius was adopted from a preliminary value that one of us (DJT) provided in the early stages of analyzing speckle interferometry data. This orbital radius differs slightly from the final value of 19,640 km (Beletic *et al.* 1989) and will have little effect on the model values.

TABLE IV

SPOT MODEL PARAMETERS FOR MAX

	Radius (km)	w	P(0)		
Pluto[a]	*1162.0*	0.789	2.4		
Charon[b]	*620.7*	*0.863*	*1.*		
Spot	Latitude	Longitude	Radius	w	P(0)
#1	−13.9	99.1	31.0	0.064	2.6
#2	−25.9	315.7	17.4	0.142	1.4
#3	79.6	213.4	62.4	1.000	1.3
#4	*South Pole*		45.3	1.000	1.5

Note. Both radii are based upon an assumed orbital radius of 19,800 km.
[a] Numbers on this line are unspotted properties of Pluto.
[b] Numbers for Charon are global properties.

TABLE V

MODEL FIT SUMMARY

Year	Points	χ^2	χ_r	$\overline{\lvert O-C \rvert}$	$\bar{\sigma}$	$\overline{O-C}$
		SHELF		Total $\chi^2 = 1768$		
1954 w	6	17.4	1.76	0.0067	0.0058	−0.0028
1955 wh	15	80.1	2.39	0.0083	0.0070	−0.0047
1964 h	14	77.2	2.43	0.0137	0.0097	0.0081
1972 a	18	88.4	2.29	0.0358	0.0242	0.0311
1975 lnf	12	8.0	0.84	0.0302	0.0483	−0.0071
1980 tt	26	98.9	2.02	0.0075	0.0052	0.0030
1981 tt	35	292.9	2.99	0.0079	0.0041	0.0001
1982 bm	27	326.6	3.59	0.0171	0.0080	−0.0050
1982 t	17	297.6	4.32	0.0113	0.0039	0.0091
1983 bm	57	112.0	1.45	0.0091	0.0079	−0.0074
1983 t	20	71.8	1.96	0.0039	0.0031	−0.0001
1984 bm	27	100.9	2.00	0.0127	0.0096	−0.0012
1986 t	44	195.9	2.18	0.0073	0.0047	0.0043
		MAX		Total $\chi^2 = 1844$		
1954 w	6	19.1	1.84	0.0078	0.0058	−0.0032
1955 wh	15	107.2	2.76	0.0087	0.0070	−0.0063
1964 h	14	91.2	2.64	0.0139	0.0097	0.0095
1972 a	18	92.2	2.34	0.0366	0.0242	0.0330
1975 lnf	12	8.1	0.85	0.0312	0.0483	−0.0064
1980 tt	26	99.7	2.02	0.0071	0.0052	0.0038
1981 tt	35	360.6	3.32	0.0083	0.0041	−0.0007
1982 bm	27	227.2	3.00	0.0157	0.0080	−0.0031
1982 t	17	341.1	4.63	0.0107	0.0039	0.0101
1983 bm	57	157.5	1.72	0.0099	0.0079	−0.0076
1983 t	20	76.7	2.02	0.0038	0.0031	−0.0001
1984 bm	27	87.9	1.86	0.0124	0.0096	−0.0016
1986 t	44	175.8	2.07	0.0072	0.0047	0.0020

Note. 1° resolution surface integral.

In the early stages of the modeling, the centers of both polar caps were fixed on the poles. With an early limitation that prevented overlapping spots, we were unable to make the dark equatorial spot large enough. To remedy this difficulty, we allowed the polar caps to slip off of the pole thereby allowing more room for the dark spot to "grow." We found that the south polar cap did not move far from the pole but the north polar cap moved off by a substantial amount. In an effort to eliminate unnecessary free parameters, we fixed the center of the south polar cap exactly on the pole thus reducing the number of free parameters to 22, while allowing the position of the north cap to vary. Later improvements to the modeling software eliminated the overlapping spot restriction, but we have not tried to recenter the north polar cap on the pole.

The fits to individual data sets for the two models are summarized in Table V. The letters shown after the year are the first letters from the last names of the observers tabulated in Table II. The column labeled χ_r provides a check on the fit in units of a standard deviation. A perfect fit given the stated errors would yield $\chi_r = 1$. A value of 2 could indicate the error bars were underestimated by a factor of 2. The scatter of the fit is tabulated under $\overline{|O-C|}$ while the mean error is shown under $\overline{O-C}$. If these two quantities are equal and larger than the mean error bar ($\bar{\sigma}$), then the model differs systematically from the data.

In Fig. 4, a subset of the data is plotted against the model calculations for the SHELF model. The agreement between the model and the data is typical of the fit to the other data sets. The scatter in the fit is 0.0078, 0.0137, and 0.0073 mag for 1954–1955, 1964, and 1986, respectively. Figure 5 shows the agreement between both sets of model parameters and the orbital lightcurve. Again, the differences between the fit given by SHELF and MAX are negligible.

Within the data set, the poorest fit (using SHELF) is to the data from 1971 to 1975 with a scatter of 0.0336 mag while the best fit occurs for the 1983 Tholen data with a scatter of 0.0039. The fit to the data from

TABLE VI

ERROR ANALYSIS FOR SHELF

Description of Parameter		Linear† $2\chi^2$			
Pluto background w		0.16			
Pluto background P(0)		0.81			
Spot	Latitude	Longitude	Radius	w	P(0)
#1	4.3	15.6	0.6	5.52	18.9
#2	15.3	4.2	0.8	5.87	30.5
#3	0.5	5.7	2.0	0.30	5.4
#4	...	...	3.1	0.03	31.9

† See text for a description of this quantity.

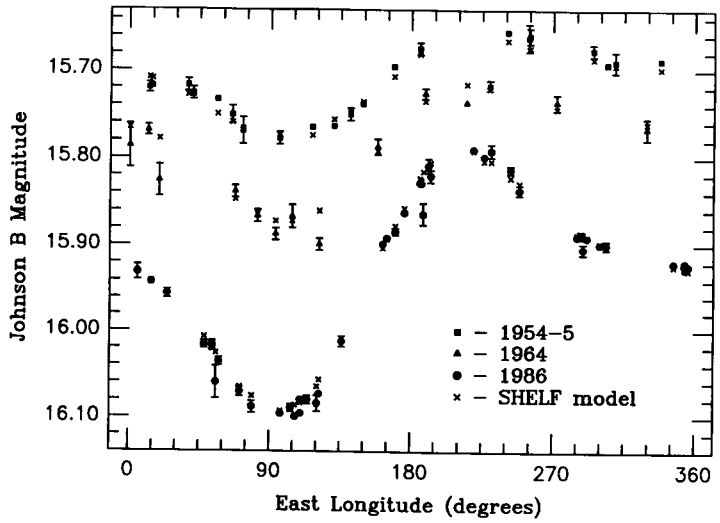

FIG. 4. Best fit to the photometry using four spots. The starting point for the least-squares fit was SHELF. In most cases the model magnitude is indistinguishable from the data. Points with error bars are data. The x's represent the model. For clarity, all uncertainties less than 0.004 mag are not shown.

the MAX model is very similar. The total χ^2 is 1768 and 1844 for SHELF and MAX, respectively, while the square root of the reduced χ^2 (χ_r) is 2.436 and 2.488. There are no systematic trends in χ_r with the different data sets and we feel confident that our error bars are not underestimated by a factor of 2 as is indicated by χ_r. Therefore we conclude that the excess scatter is caused by something other than the random errors. One possibility is that we are seeing the effects of systematic differences between the six photometric systems used by the various observers at the level at which the model is now fitting the data.

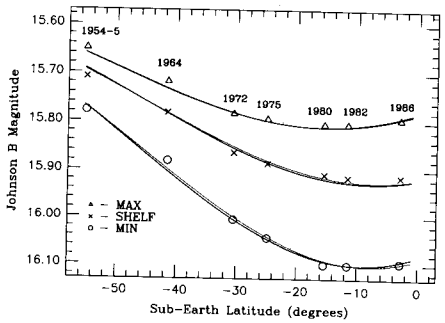

FIG. 5. Comparison between the orbital lightcurve and both the SHELF and the MAX model curves. Both models reproduce the orbital lightcurve very well.

Table VI represents our best efforts toward determining uncertainties for the derived model parameters. Each number in this table represents an estimate of the change in that free parameter that is needed in order to double the χ^2. To determine an error bar for a given parameter, we perturbed that parameter from its nominal value. The remaining 19 free parameters were then adjusted by the simplex program to try and minimize the χ^2 again. The two values for the perturbed parameter with their associated χ^2 serve to define the curvature of the χ^2 surface for that parameter. To save on computer time, only one point in a single direction from the nominal value was computed and the computation was done at 3° resolution. While these numbers do not reflect a standard uncertainty, they give one a feel for the relative importance of each parameter in the model fit. Not surprisingly, a few parameters have uncertainties that are quite large. $P(0)$ for all of the spots, w for the equatorial spots, the longitude of the dark equatorial spot, and the latitude of the bright equatorial spot are the

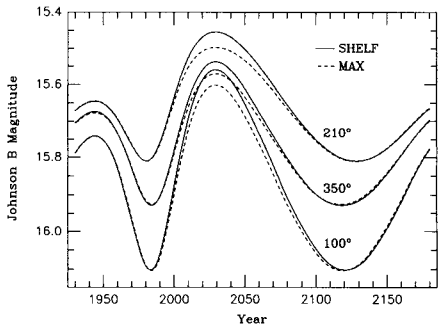

FIG. 6. Plot of the orbital lightcurve predicted by both models for one full Plutonian year. It will be a great many years before out-of-eclipse photometry can distinguish between the two models.

most poorly determined quantities. Some of the values seem to be very tightly constrained. In particular, the uncertainties on the radii of the spots are quite low.

On the basis of the fit to the available out-of-eclipse photometry, MAX and SHELF work equally well in explaining the known lightcurve behavior of Pluto. Figure 6 shows the predicted orbital lightcurves for a complete orbit of Pluto around the Sun. It is no surprise that the models agree quite well in the time span constrained by data. The models do not diverge very fast beyond the last constraint in 1986. Figure 7 shows the rotational lightcurve for a few different times. The four curves labeled 1950 through 1980 show the observed evolution of the lightcurve where the two models do not differ strongly. However, the plot for 2020 shows a strong difference between the models.

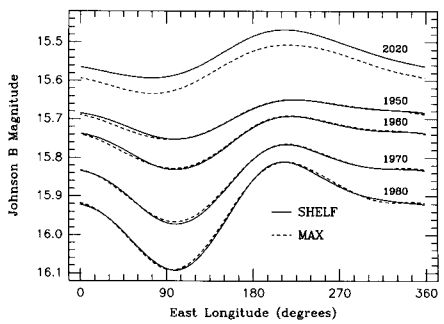

FIG. 7. Rotational lightcurves from the SHELF (solid lines) and MAX model (dashed lines) for selected epochs. Each plot represents the brightness of Pluto during a single rotation at the time of opposition for the indicated year.

(Note that in the curves for SHELF in Fig. 7, the lightcurve minimum from 1950 to 1980 remains at the same longitude while the lightcurve maximum drifts from 225° in 1950 to 210° in 1980. This drift is precisely the behavior we expected that would perturb the determination of a lightcurve period from the out-of-eclipse photometry.)

From these plots it is clear that we would need to wait a very long time to eliminate one of the two models on the basis of lightcurve photometry alone. Fortunately, the mutual events can decide the question much sooner. Through the end of 1987, both models predict nearly identical event lightcurves. The similarity arises because the models do not differ on the Charon-facing hemisphere in the northern hemisphere and the satellite transit events have been progressing from the north pole to the south. Thus, the model lightcurves do not differ until the satellite begins to cover material at the latitude of spot #2 in the MAX model, that is, southward of $-8°$ lat.

Our first observation of an inferior event this far south occurred on 1988 January 13 UT. The data from this observation are shown in Fig. 8. The solid curve, referred to as "three circles," is based on the uniform albedo model we have been using to model the orbit and sizes of Pluto and Charon. This model is discussed more fully in Tholen *et al.* (1987). The three-circle model does not model the effects of the background lightcurve and has been shifted vertically to match the data. On the other hand, the spot model provides both the overall brightness of Pluto and Charon as well as the brightness of the system during an event. For this reason, no shifts or corrections are necessary, or appropriate, for the SHELF and MAX curves. Upon close examination, we find that the MAX model predicts a much later minimum and more

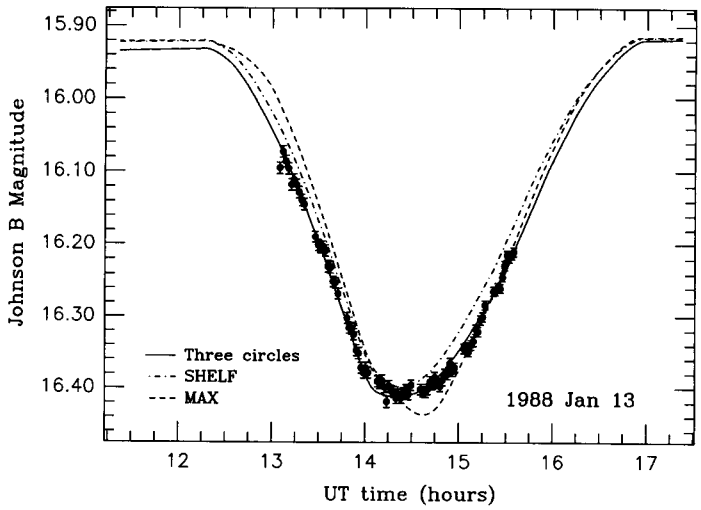

FIG. 8. New constraints provided by the mutual events. Of the two models presented here, only SHELF is consistent with this transit lightcurve. On the basis of this plot, we have ruled out MAX as a viable surface albedo distribution. Other than visual inspection, these data have not been used to constrain either the MAX or the SHELF models.

asymmetric lightcurve than is shown by the data. The SHELF model, which has no longitudinal albedo markings on the Charon-facing hemisphere, matches the data quite closely. Aside from a small vertical shift, SHELF and the three-circle model are nearly identical. From this comparison, we find that the MAX model is inconsistent with the mutual event data and can now be dismissed.

To help visualize the Pluto albedo map, we have generated images from the model. These pictures are shown in Fig. 9. This set of images represents the most realistic image that we can generate at this time. The limb-darkening evident in the images (except for Charon) is a natural consequence of the Hapke formula. The shadowing of the surface of Pluto does *not* represent a circular approximation. The shape comes from a full geometric computation for each point on the surface. It is interesting to note, however, that the shadow does appear to be circular, vindicating our assumptions in using the three-circle approach elsewhere. For a better feel of the reflectance of the surface, Fig. 10 shows center-to-limb reflectance values for the different albedo domains on Pluto. As Figs. 9 and 10 show, the albedo of the surface of Pluto varies a great deal. In fact, the contrast ratios are much greater than Marcialis' 2 : 1 assumption for the equatorial spots.

DISCUSSION

One of the basic questions we set out to investigate was whether a static surface albedo distribution could reproduce Pluto's observed lightcurve behavior. Originally Marcialis (1983) and more recently Stern *et al.* (1988) have argued in favor of a dynamic albedo distribution on time scales that are short compared to the orbital period of Pluto. Stern *et al.*'s primary arguments in favor of this conclusion are the rapid dimming of Pluto as it approaches perihelion, a simultaneous reddening of the planet, and the extremely high albedo, which implies a very fresh frost deposit.

We have shown that a fixed albedo distribution can also reproduce the rapid dimming of Pluto as it approaches perihelion. The reddening discussed by Stern *et al.* is by no means confirmed. Our own observations now span 1980 to the present and no color change has occurred, yet our $(B - V)$ color is slightly redder than earlier, but less precise, measurements; the significance is

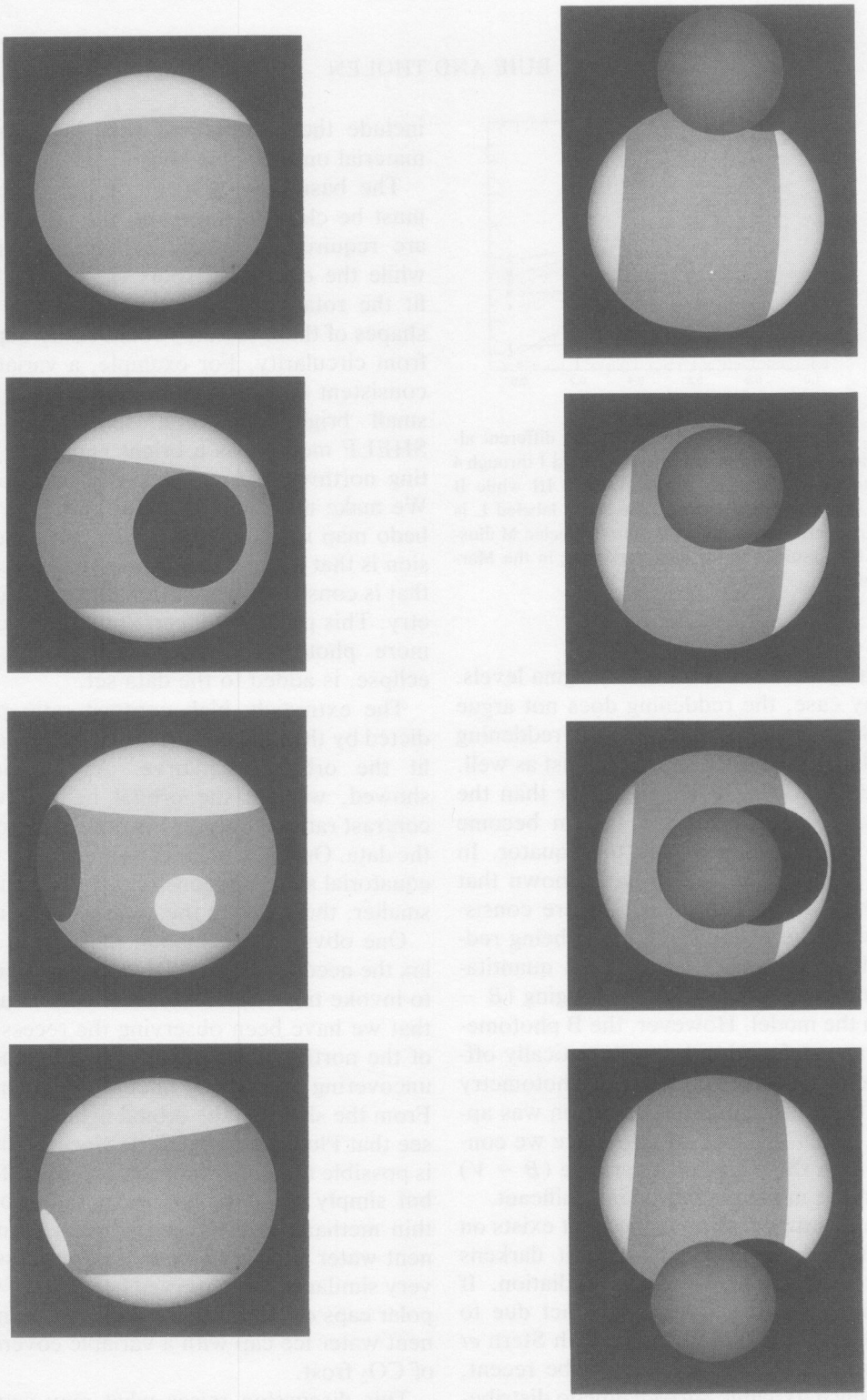

FIG. 9. A computer-generated picture of Pluto, SHELF model. The left panel depicts four different equatorial views of Pluto, from top to bottom, 0°, 90°, 180°, and 270°. Pluto's north appears at the top. The right panel shows four views during the 1987 March 19 transit of Charon in front of Pluto. The orientation matches how we see Pluto from Earth. Our north is at the top in these pictures; Pluto's north pole is to the right. This sequence covers roughly 4 hr going from the top frame to the bottom.

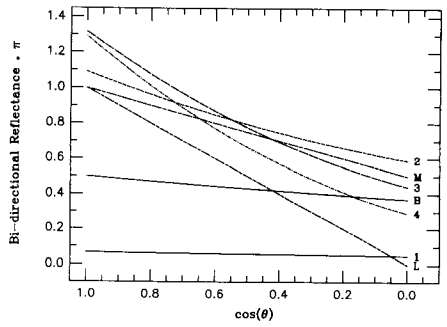

FIG. 10. Center-to-limb profiles of the different albedo domains on Pluto. The curves labeled 1 through 4 refer to the spots as indicated in Table III while B refers to the equatorial band. The curve labeled L is for a Lambertian sphere and the curve labeled M illustrates the assumed linear limb-darkening in the Marcialis model.

probably between the 1 and 2 sigma levels. In any case, the reddening does not argue for Stern *et al.*'s model since reddening could occur with a static model just as well. If the equatorial region is redder than the poles, we would see the system become more red as we approach the equator. In fact, Binzel *et al.* (1988) have shown that the mutual event observations are consistent with the equatorial regions being redder than the poles. We did not quantitatively analyze the effect of changing $(B - V)$ on the model. However, the B photometry was not found to be systematically offset from the offset from the V photometry once the constant color correction was applied. From this lack of difference we conclude that the effect of a variable $(B - V)$ within the model would be insignificant.

We do know that methane frost exists on the surface of Pluto and that it darkens when exposed to ultraviolet radiation. If the high albedo of Pluto is in fact due to methane frost, then we agree with Stern *et al.* that the frost deposits must be recent, implying a dynamic surface albedo distribution. However, we note that Enceladus also has a very high albedo surface, similar in albedo to the bright regions on Pluto. The difficulty with any mechanism that generates bright surfaces will be how one can include the presence of very low albedo material on the same body.

The basic arrangement of the "spots" must be close to the truth; the polar caps are required to fit the orbital lightcurve while the equatorial spots are required to fit the rotational lightcurve, although the shapes of these features could easily depart from circularity. For example, a variation consistent with this model could be if the small bright equatorial spot from the SHELF model was a bright peninsula jutting northward from the south polar cap. We make no claims that this particular albedo map is unique. Our principle conclusion is that a static map *can* be constructed that is consistent with all available photometry. This picture will certainly improve as more photometry, both in and out of eclipse, is added to the data set.

The extremely high contrast ratio predicted by the model is driven by the need to fit the orbital lightcurve. As Marcialis showed, without the orbital lightcurve a contrast ratio of only 2 : 1 is necessary to fit the data. Once the polar caps are added, the equatorial spots are constrained to be much smaller, thus driving the contrast ratio up.

One obvious explanation that would relax the need for such a high contrast ratio is to invoke time variability. It is conceivable that we have been observing the recession of the north polar cap and the subsequent uncovering of a darker underlying surface. From the shape of the orbital lightcurve we see that Pluto has faded little since 1980. It is possible that this is not a geometric effect but simply the complete evaporation of a thin methane frost layer leaving a permanent water ice cap in view. This process is very similar to the observed behavior of the polar caps on Mars where there is a permanent water ice cap with a variable covering of CO_2 frost.

This discussion raises what may sound like completely open questions that may never be solved but the mutual events between Pluto and Charon will be able to provide some additional constraints. The first of the 1988 satellite transits has already pro-

vided a direct discrimination between the two models presented here. Once we have a full set of transits covering the entire hemisphere of Pluto, we should be able to improve substantially on the albedo map derived here. The time span of the mutual events is short enough that any temporal variation will have a marginal effect on the modeling. Combining event observations and the rest of the out-of-eclipse measurements, we should be able to decide whether or not there have been significant temporal variations on the Pluto surface.

We would like to stress the importance of monitoring the out-of-eclipse brightness of Pluto with high precision photometry ($\sigma <$ 0.005 mag) during and after the mutual event season. It is very important to get a well-sampled lightcurve, especially the maximum and minimum. Not only will continued lightcurve photometry aid the analysis of the mutual event data, but it will also continue to be important as we strive to improve our limited knowledge of the surface of Pluto.

ACKNOWLEDGMENTS

This research was supported by the San Diego Supercomputer Center through the University of Hawaii block grant and NASA Grant NGL 12-001-057. Special thanks go to Steve Lamont, Mark Sheddon, and Mike Keeler for their help with the computer graphics at SDSC. We also thank Jay Goguen and John Spencer for algorithmic insights, Neil Lark for his assistance on the night of 1986 March 6, Rick Binzel for providing his complete Pluto data set in digital form, and Ewen Whitaker for digging through the Kuiper archives in search of the lost Pluto photometry.

REFERENCES

ABRAMENKO, A. N., V. V. AVRAMCHUK, V. A. KUCHEROV, L. R. LISINA, AND V. V. PROKOFIEVA 1981. The reflective properties of Pluto's surface. In *Physics of Planetary Atmospheres* (A. V. Morozhenko, Ed.), pp. 148–157. Academy of Sciences, Kiev.

ANDERSSON, L. E., AND J. D. FIX 1973. Pluto: New photometry and a determination of the axis of rotation. *Icarus* **20,** 279–283.

Astronomical Almanac for the Year 1988, The. U.S. Government Printing Office, Washington, DC.

BAADE, W. 1934. The photographic magnitude and color index of Pluto. *Publ. Astron. Soc. Pac.* **46,** 218–221.

BELETIC, J. W., R. M. GOODY, AND D. J. THOLEN 1989. Orbital elements of Charon from speckle interferometry. *Icarus* In press.

BINZEL, R. P., M. L. FRUEH, AND J. D. MULHOLLAND 1988. Pluto–Charon mutual events: A midseason report. *Bull. Amer. Astron. Soc.* **19,** 1071.

BINZEL, R. P., AND J. D. MULHOLLAND 1984. Photometry of Pluto during the 1983 opposition: A new determination of the phase coefficient. *Astron. J.* **89,** 1759–1761.

CACECI, M. S., AND W. P. CACERIS 1984. Fitting curves to data. *Byte* **9,** 340–362.

HAPKE, B. 1981. Bidirectional reflectance spectroscopy. 1. Theory. *J. Geophys. Res.* **86,** 3039–3054.

HARDIE, R. H. 1965. A re-examination of the light variation of Pluto. *Astron. J.* **70,** 140.

HARRINGTON, R. S., AND J. W. CHRISTY 1981. The satellite of Pluto. III. *Astron. J.* **86,** 442–443.

KILADZE, R. I. 1966. On the rotation period of Pluto. *Bull. Abastumani. Astrophys. Obs.* **34,** 131–133.

KILADZE, R. I. 1967. Physical parameters of Pluto. *Sol. Sys. Res.* **1,** 173–175.

LACIS, A. A., AND J. D. FIX 1972. An analysis of the light curve of Pluto. *Astrophys. J.* **174,** 449–453.

LANE, W. A., J. S. NEFF, AND J. D. FIX 1976. A measurement of the relative reflectance of Pluto at 0.86 microns. *Publ. Astron. Soc. Pac.* **88,** 77–79.

LYUTYI, V. M., AND V. P. TARASHCHUK 1982. A photometric study of Pluto near perihelion. I. U, B, V photometry. *Sov. Astron. Lett.* **8,** 56–59.

MARCIALIS, R. L. 1983. *A Two-Spot Model for the Surface of Pluto.* M.S. thesis. Vanderbilt University, Nashville, TN.

MARCIALIS, R. L. 1988. A two-spot albedo model for the surface of Pluto. *Astron. J.* **95,** 941–947.

NEFF, J. S., W. A. LANE, AND J. D. FIX 1974. An investigation of the rotational period of the planet Pluto. *Publ. Astron. Soc. Pac.* **86,** 225–230.

RENSCHEN, C. P. 1977. An interpretation of Pluto's light variation. *Astron. Nachr.* **298,** 179–184.

STERN, S. A., L. M. TRAFTON, AND G. R. GLADSTONE 1988. Why is Pluto bright? Implications of the albedo and lightcurve behavior of Pluto. *Icarus* **75,** 485–498.

THOLEN, D. J. 1985. Pluto–Charon mutual event predictions for 1986. *Astron. J.* **90,** 2639–2642.

THOLEN, D. J., AND M. W. BUIE 1987. Pluto and Charon: Radii, density, and orbital elements from mutual event photometry through 1987. *Bull. Amer. Astron. Soc.* **19,** 859.

THOLEN, D. J., M. W. BUIE, R. P. BINZEL, AND M. L. FRUEH 1987. Improved orbital and physical parameters for the Pluto–Charon system. *Science* **237,** 512–514.

THOLEN, D. J., AND E. F. TEDESCO 1989. Pluto's lightcurve: Results from four apparitions, in preparation.

WALKER, M. F., AND R. HARDIE 1955. A photometric determination of the rotational period of Pluto. *Publ. Astron. Soc. Pac.* **67,** 224–231.